Submitted to

31st International Conference on High Energy Physics, ICHEP02, July 24, 2002, Amsterdam
Abstract: **1009**
Parallel Session **5**

www-h1.desy.de/h1/www/publications/conf/conf_list.html

Measurement of dijet cross-sections at low Q^2 at HERA

H1 Collaboration

Abstract

Triple differential dijet cross-sections in $e^{\pm}p$ interactions measured with the H1 detector at HERA are presented in the region of photon virtualities $2\ \mathrm{GeV}^2 < Q^2 < 80\ \mathrm{GeV}^2$, inelasticities $0.1 < y < 0.85$, low transverse jet momentum $E_t^{jet\,1,2} > 5$ GeV with average $\overline{E}_t > 6$ GeV, and pseudorapidity $-2.5 < \eta^{jet\,1,2} < 0$. The data are compared to Monte Carlo simulations which differ in their assumptions about the virtual photon structure and employ DGLAP or CCFM parton evolution schemes. Indications of effects connected with the interaction of longitudinally polarized virtual photons via their resolved hadronic structure are investigated.

1 Dijet Production at HERA

The production of dijet events at HERA is dominated by processes in which a virtual photon, coupling to the electron, interacts with a parton in the proton. If the mediated photon is almost real ($Q^2 < \Lambda^2_{QCD}$), the data are usually described by the sum of two types of process. In the "direct" case, the photon interacts as a whole with partons from the proton, while in the "resolved" interaction, the photon behaves as a hadron, i.e. as a source of partons described by set of parton distribution functions (PDF). The same approach has been applied in LO models in the past to virtual photons with $Q^2 < E_t^2$. The resolved contributions seem to be present in data [1, 2, 3, 4]. However, contrary to the photoproduction regime, we are not obliged to introduce the concept of resolved photons if $Q^2 \gg \Lambda^2_{QCD}$. Since leading order direct interactions are not able to fully describe the data in the region of virtuality $\Lambda^2_{QCD} \ll Q^2 \lesssim E_t^2$ explored in the present analysis, higher order effects need to be included in some way – either using next-to-leading order (NLO) calculations, via k_t unordered initial QCD cascades, or by allowing for additional interactions with resolved photons. Only the last two approaches are investigated here. Comparisons with NLO predictions are likely to become possible in the future. In more detail, the present measurements are compared with the following models:

a) LO direct and resolved interactions based on the DGLAP evolution equations and parton showers. The effects of transversally (γ_T^*) and also longitudinally (γ_L^*) polarized resolved photon interactions are included [5, 6, 7]. The cross section for longitudinal photons vanishes for $Q^2 = 0$ due to gauge invariance. On the other hand, the concept of a resolved photon breaks down for $Q^2 > E_t^2$. Therefore the most promising region in which to search for the γ_L^* resolved processes is $\Lambda^2_{QCD} < Q^2 \ll E_t^2$, which is often the case of the present analysis.

The main difference between γ_L^* and γ_T^* induced interactions arises from the y dependence of the respective fluxes:

$$f_{\gamma^T/e}(y, Q^2) = \frac{\alpha}{2\pi}\left[\frac{2(1-y)+y^2}{y}\frac{1}{Q^2} - \frac{2m_e^2 y}{Q^4}\right] \quad (1)$$

$$f_{\gamma^L/e}(y, Q^2) = \frac{\alpha}{2\pi}\left[\frac{2(1-y)}{y}\frac{1}{Q^2}\right] \quad (2)$$

where α is the fine structure constant and m_e the electron mass. While for $y \to 0$, both transverse and longitudinal fluxes are approximately the same, the longitudinal flux vanishes for $y \to 1$. Also the dependence of the point-like [1] (i.e. perturbatively calculable) parts of the photon PDF on Q^2 and E_t^2 differs – while the γ_T^* PDF are proportional to $\ln(E_t^2/Q^2)$, the γ_L^* PDF do not, in the first approximation, depend on either E_t^2 or Q^2 [6].

Monte Carlo programs HERWIG 5.9 [9] and RAPGAP 2.8 [10] based on the DGLAP evolution scheme were chosen for comparisons with the data. These models differ in the choice hadronization model – a cluster fragmentation is applied in HERWIG, the Lund string model in RAPGAP. Neither of the two programs include the resolved interaction of γ_L^*. For this purpose

[1] The perturbatively non-calculable hadron-like part of the photon PDF becomes negligible in our kinematical region with respect to the point-like one, as has been demonstrated in [8].

we used a slightly modified version of HERWIG with the longitudinal photon flux according to eq. (2) and a recent γ_L^* PDF parameterization [7].

b) k_t unordered initial QCD cascades accompanying the hard process are present for example in BFKL or CCFM evolution. These evolution schemes can lead to final states in which the partons with the largest k_t may come from the cascade, and not, as in the DGLAP case, from the hard subprocess. Such events may have a similar topology to that for the resolved interactions in the DGLAP approximation. This possibility is investigated using the CASCADE 1.0 generator [11, 12] based on the CCFM evolution equations and unintegrated gluon density functions [13]. Contrary to DGLAP models, resolved photons are not considered in CASCADE.

2 Measurement of Dijet Cross-Section

The measurement was done with 16.3 pb^{-1} of data collected in 1999, when the electron-proton center-of-mass energy $\sqrt{s}$ reached 318 GeV. A full description of the H1 detector is given in [14, 15].

The kinematic variables x, Q^2 and y are determined from the electron information only, according to $Q^2 = 4E_eE'_e\cos^2(\theta_e/2)$, $y = 1-(E_e/E'_e)\sin^2(\theta_e/2)$ and $x = Q^2/(ys)$, where E_e, E'_e and θ_e are the electron beam energy, the energy of the scattered electron and the electron scattering angle, respectively.

The analysis was performed in γ^*-proton center-of-mass system, and jets were found using the k_t longitudinally invariant jet algorithm. The phase space is defined by the photon virtuality: $2\ \mathrm{GeV}^2 < Q^2 < 80\ \mathrm{GeV}^2$, the electron inelasticity: $0.1 < y < 0.85$, the transverse energy of two leading jets: $E_t^{jet\,1,2} > 5$ GeV, $\overline{E}_t = (E_t^{jet\,1} + E_t^{jet\,2})/2 > 6$ GeV and the pseudorapidity of the two leading jets: $-2.5 < \eta^{jet\,1,2} < 0$. The E_t^{jet} and η^{jet} variables are measured relative to the γ^*p collision axis with positive η^{jet} corresponding to the proton direction.

The dijet events are characterized by $\overline{E}_t^2$, which is the mean value of transverse energy E_t of two jets with the highest E_t, and in terms of the variable x_γ defined as:

$$x_\gamma = \frac{\sum\limits_{\text{jet 1,2}} (E^{jet} - p_z^{jet})}{\sum\limits_{\text{hadrons}} (E - p_z)} \tag{3}$$

For a $2 \to 2$ process involving four massless partons, the above expression gives exactly the fraction of the photon momentum carried by the parton entering this process from the photon side. For hadronic jets, x_γ has only approximately such an interpretation, but still allows us to separate direct ($x_\gamma \sim 1$) and resolved ($x_\gamma < 1$) components with reasonable accuracy.

The measured data are corrected for the effects of limited detector acceptance and resolution using the Bayesian unfolding method. The distributions of kinematic variables (Fig. 1) and jet observables (Fig. 2) are sufficiently well described by HERWIG and RAPGAP, which were used in the correction procedure. The largest source of systematic errors, typically 10-20%, arises from the model dependence of the detector correction, which was taken as half of the difference between HERWIG and RAPGAP. Another 10% error appears due to a 4% energy scale uncertainty of the main calorimeter.

3 Results and Discussion

The corrected triple-differential dijet cross-section measured as a function of Q^2 , $\overline{E}_t^2$ and x_γ is shown in Fig. 3-7, where different model predictions are compared always to the same data points.

A prediction of HERWIG and RAPGAP with the SaS1D [16] parameterization of the γ_T^* PDF, as well as the pure direct contributions are compared to the data in Fig. 3. In general, HERWIG and RAPGAP tend to underestimate the measured cross-section. The decrease of the resolved contribution at high $\overline{E}_t^2$ is of kinematic origin, due to the limited energy of the incoming partons at low x_γ . The direct contributions almost describe the data in the highest Q^2 bin, while a clear need for resolved processes is observed for $Q^2 \ll \overline{E}_t^2$.

In the highest Q^2 range ($25 < Q^2 < 80$ GeV^2) and $x_\gamma < 0.75$, the HERWIG direct contribution almost describes the data in the lowest $\overline{E}_t^2$ bin, but is significantly below it in the highest $\overline{E}_t^2$ bin. This indicates that the relevance of the resolved photon contribution is governed by the ratio $\overline{E}_t^2/Q^2$, rather than by Q^2 itself.

Standard HERWIG with direct and γ_T^* resolved contributions underestimates the data. The description is improved by adding γ_L^* resolved photon interactions, as demonstrated in Fig. 4.

On the other hand, a simple enhancement of the PDF of the γ_T^* in the resolved contribution could lead to a similar prediction as the introduction of resolved γ_L^*. This is indicated in Fig. 7, where a modified version of the GRV [17] parameterization of the real photon PDF were used for the resolved γ_T^* component. The parameter ω governs the suppression of the photon PDF relative to real photons with increasing virtuality.

To distinguish between a non-optimal choice of γ_T^* PDF and the need for resolved γ_L^*, the dijet cross-section has been studied as a function of Q^2 , x_γ and y, which is shown in Fig. 8-12. HERWIG and RAPGAP are below the data especially at low x_γ and low y (Fig. 8). The discrepancy becomes smaller if the resolved γ_L^* is added (Fig. 9). According to eq. (1-2), the slope of inelasticity y of the HERWIG prediction in the region of $x_\gamma < 0.75$ depends significantly on whether γ_L^* processes are included or not. Unlike a pure enhancement of γ_T^* PDF, which would not change the slope of the y distribution, addition of γ_L^* brings the y dependence of HERWIG much closer to the measurement (compare Fig. 9 and 12).

As motivated in Section 1, the measured cross-sections are also compared to a prediction of the CASCADE MC program based on the CCFM evolution scheme (Fig. 5 and 10). This theoretical approach does not involve the concept of virtual photon structure and employs much fewer parameters for tuning than the usual DGLAP-based MC programs. CASCADE describes the data reasonably but not perfectly. In particular, the Q^2 dependence at low x_γ is poorly described (see e.g. Fig. 11).

As indicated by Fig. 10, the y dependence of the dijet cross-section is better described by CASCADE than by HERWIG without the γ_L^* resolved process, since photon polarization states are correctly treated in CASCADE for all virtualities (only direct photon interactions are included).

In Fig. 13-17, simplified versions of Fig. 3-12 are presented, where only a part of the measured phase space is displayed.

4 Conclusions

The importance of γ_T^* resolved photon interactions within the DGLAP evolution scheme at leading order is clearly demonstrated in the region where $\overline{E}_t^2 > Q^2$, even at rather high Q^2. Additional γ_L^* resolved photon contributions further improve the agreement of HERWIG with the measured data.

Exploring the CCFM approach, the MC program CASCADE does not reproduce the data perfectly, the main discrepancy is observed in the Q^2 dependence at low x_γ. On the other hand, the x_γ dependence in CASCADE is comparable to the sum of the direct and resolved contributions in DGLAP-based MC programs, showing that non k_t ordered parton cascades can successfully produce the same observables as resolved virtual photons in the LO DGLAP evolution scheme.

References

[1] C. Adloff *et al.* [H1 Collaboration], Eur. Phys. J. C **13** (2000) 397 [arXiv:hep-ex/9812024].

[2] D. Kcira [ZEUS Collaboration], "Virtual photon structure at HERA," [arXiv:hep-ex/0110082].

[3] M. Tasevsky [H1 Collaboration], "Jets as a source of information about photon structure," [arXiv:hep-ex/9807023].

[4] S. P. Baranov, H. Jung, L. Jonsson, S. Padhi and N. P. Zotov, [arXiv:hep-ph/0203025].

[5] K. Sedlak [H1 Collaboration], "Structure of virtual photons at HERA," [arXiv:hep-ex/0111019].

[6] J. Chýla and M. Taševský, Eur. Phys. J. **C18** (2001), 723.

[7] J. Chýla, Phys. Lett. **B488** (2000), 289.

[8] J. Chýla and M. Taševský, Phys. Rev. D **62**, 114025 (2000).

[9] G. Marchesini, B.R. Webber, G. Abbiendi, I.G. Knowles, M.H. Seymour and L. Stanco, Comput. Phys. Commun. **67** (1992), 465.

[10] H. Jung, Comput. Phys. Commun. **86** (1995) 147-161.

[11] H. Jung, "The CCFM Monte Carlo Generator Cascade", Comput. Phys. Commun. **143** (2002), 100-111.

[12] H. Jung and G.P. Salam, Eur. Phys. J. **C19** (2001), 351-360.

[13] H. Jung, Phys. Rev. **D65** (2002) 034015.

[14] I. Abt *et al.* [H1 Collaboration], Nucl. Instrum. Meth. A **386** (1997) 310.

[15] I. Abt *et al.* [H1 Collaboration], Nucl. Instrum. Meth. A **386** (1997) 348.

[16] G. A. Schuler and T. Sjostrand, Z. Phys. C **68** (1995) 607 [arXiv:hep-ph/9503384].

[17] M. Drees and R. M. Godbole, Phys. Rev. D **50** (1994) 3124 [arXiv:hep-ph/9403229].

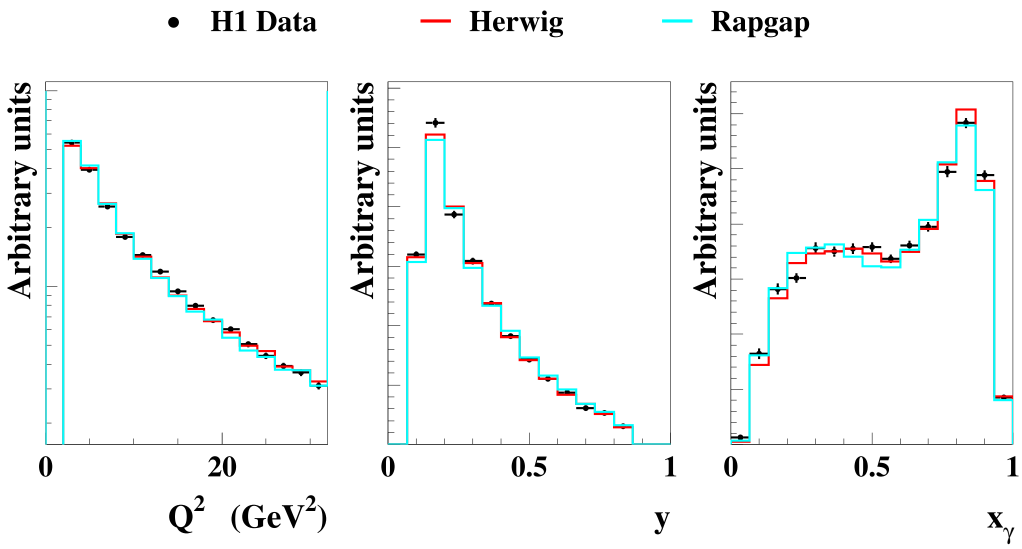

Figure 1: Detector level comparison of the data with HERWIG and RAPGAP simulations. Both HERWIG and RAPGAP are reweighted to describe the data. All detector level selection criteria were applied.

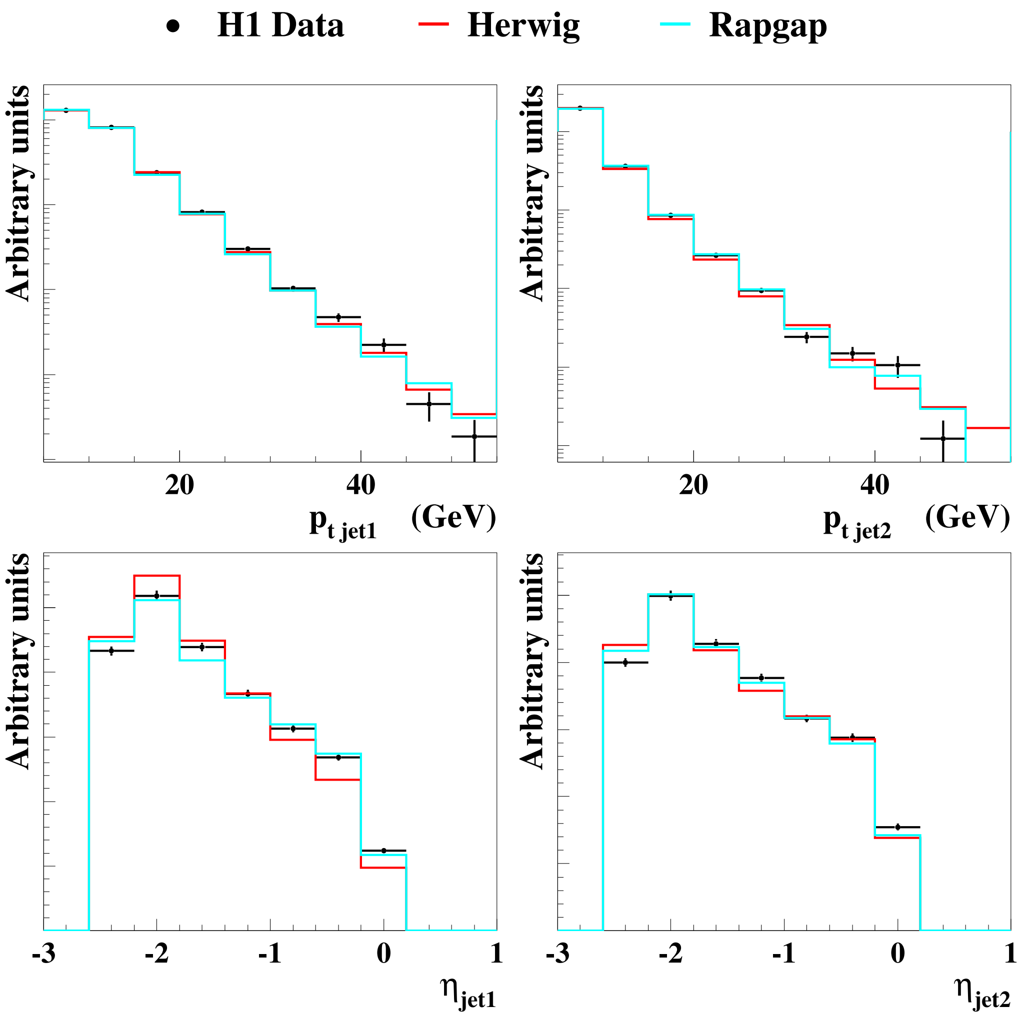

Figure 2: Detector level comparison of the data with HERWIG and RAPGAP simulations. Both HERWIG and RAPGAP are reweighted to describe the data. All detector level selection criteria were applied.

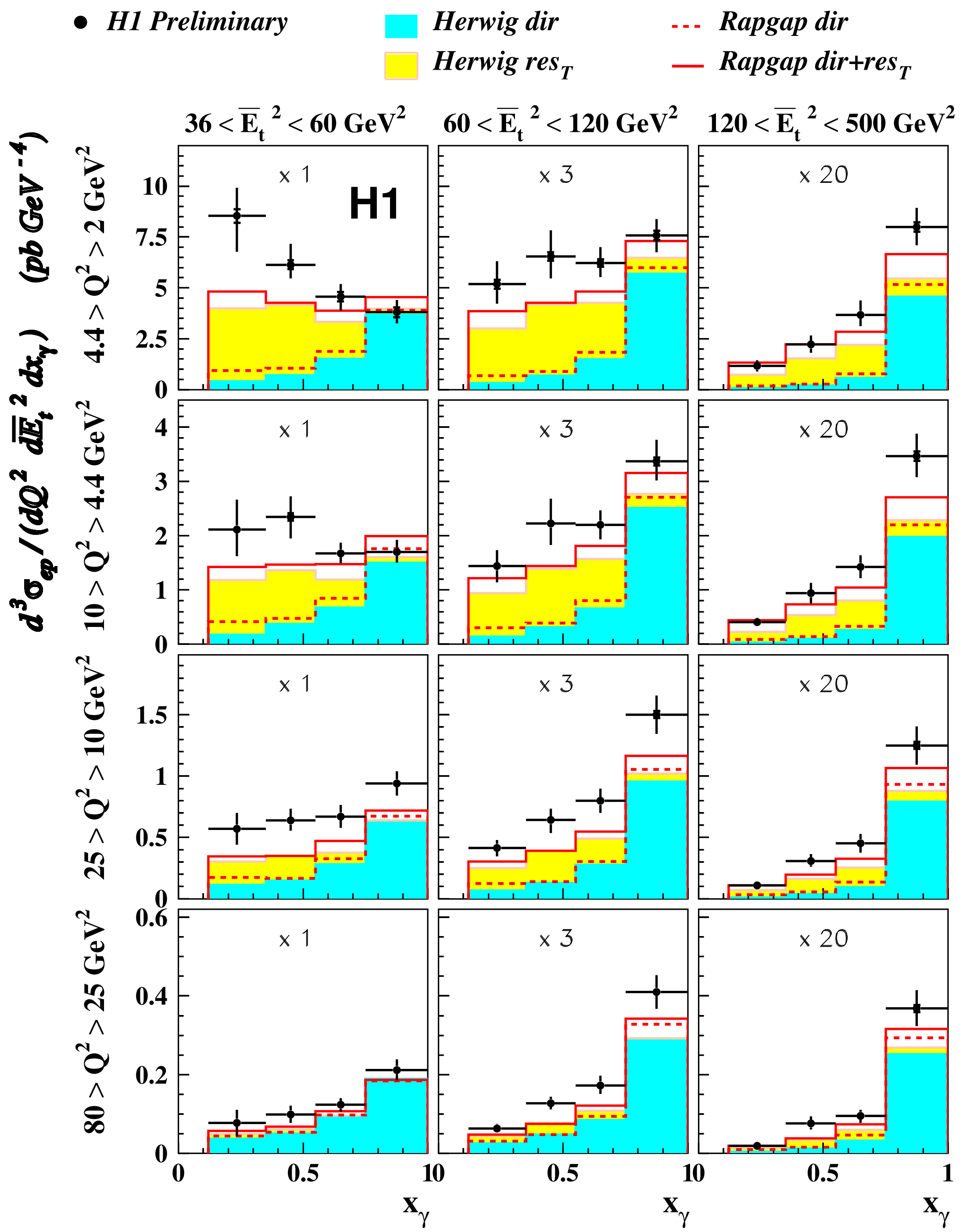

Figure 3: Triple differential dijet cross-section as a function of x_γ , $\overline{E}_t^2$ and Q^2. The data are compared to HERWIG and RAPGAP MC predictions. Separately shown are the direct (dir) and the resolved component of transversally polarized γ (res$_T$).

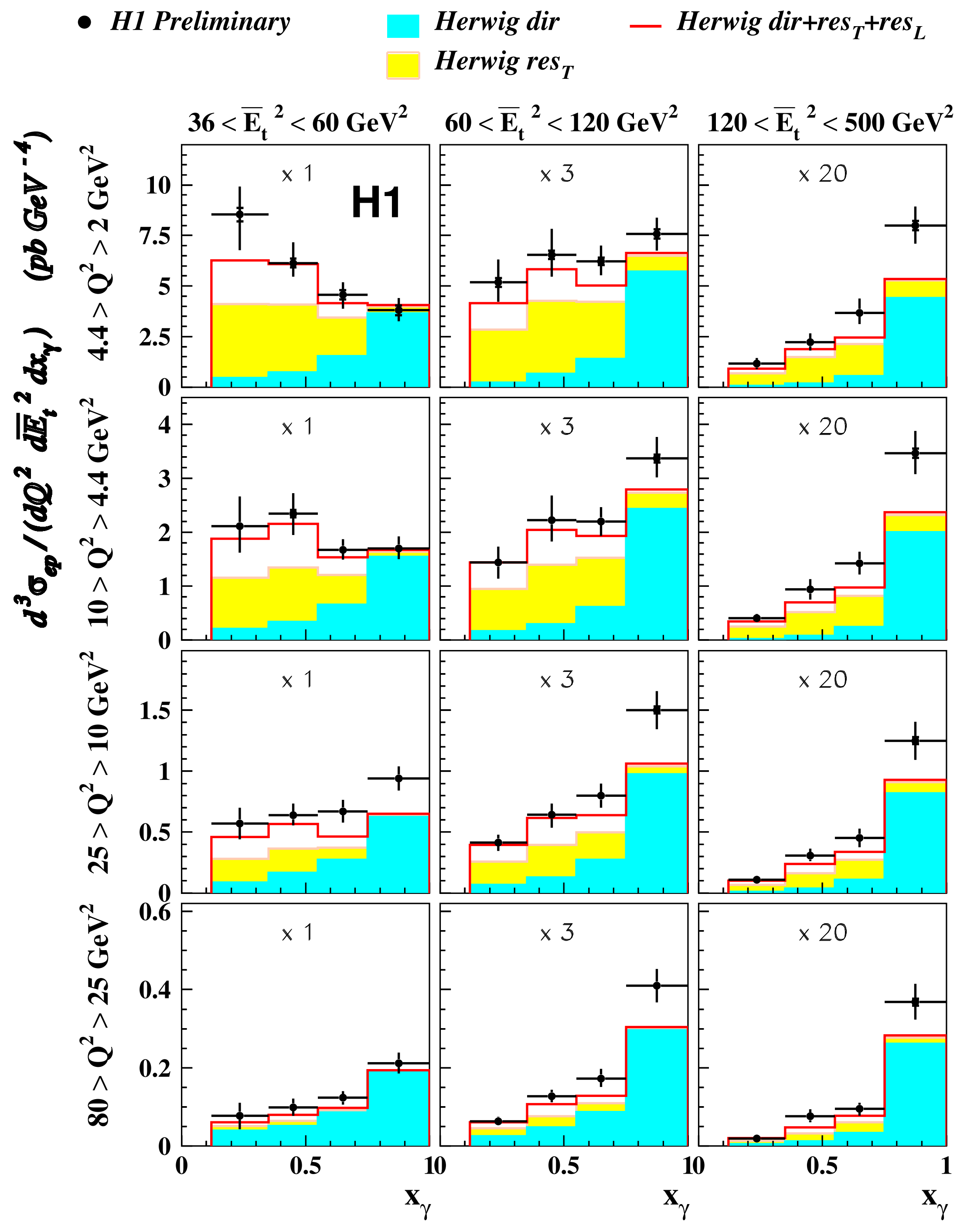

Figure 4: Triple differential dijet cross-section as a function of x_γ , $\overline{E}_t^2$ and Q^2. The data are compared to HERWIG with an additional contribution of the longitudinally polarized photon processes (res$_L$).

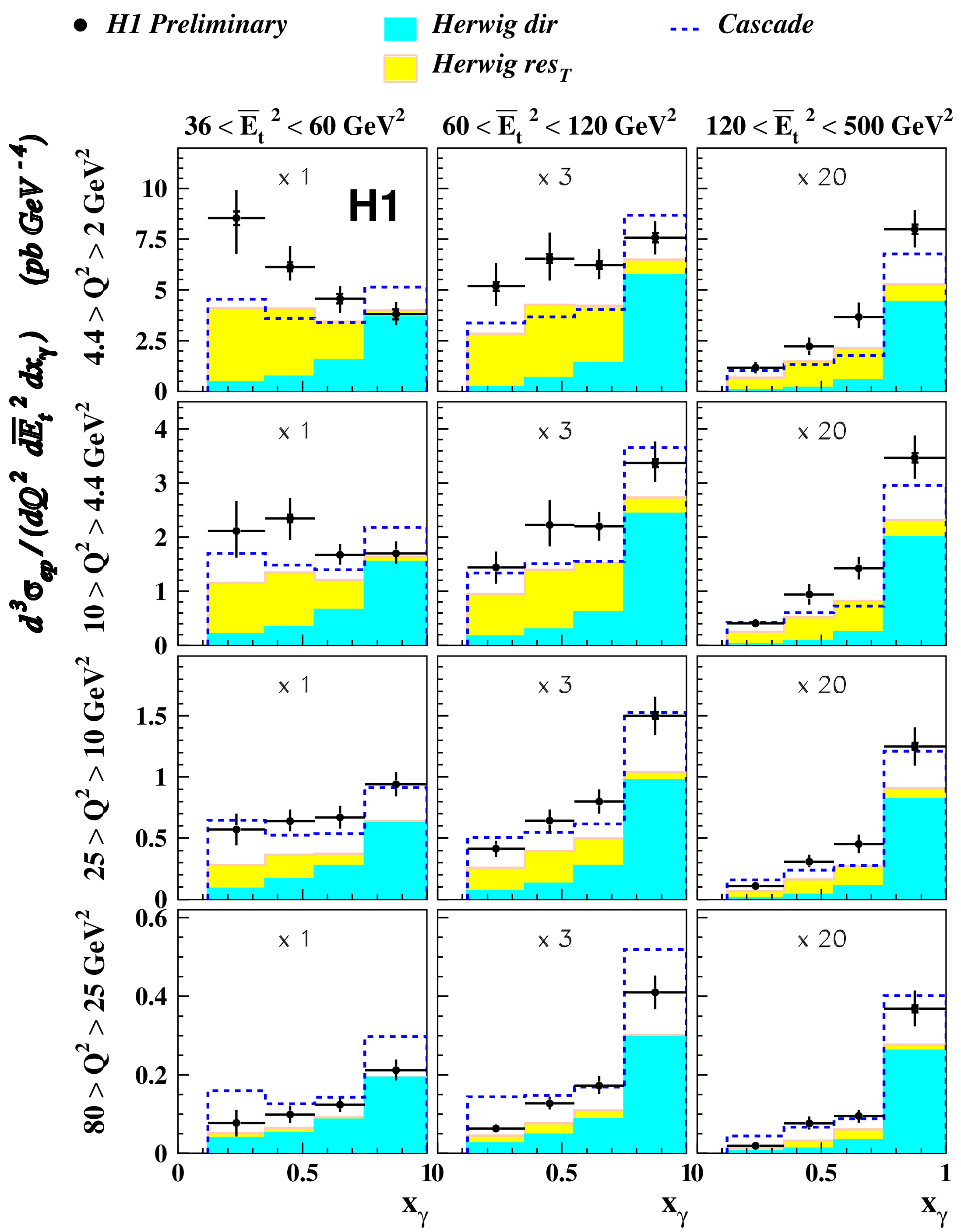

Figure 5: Triple differential dijet cross-section as a function of x_γ, $\overline{E}_t^2$ and Q^2. The data are compared to HERWIG and CASCADE MC predictions. CASCADE is based on the CCFM evolution scheme.

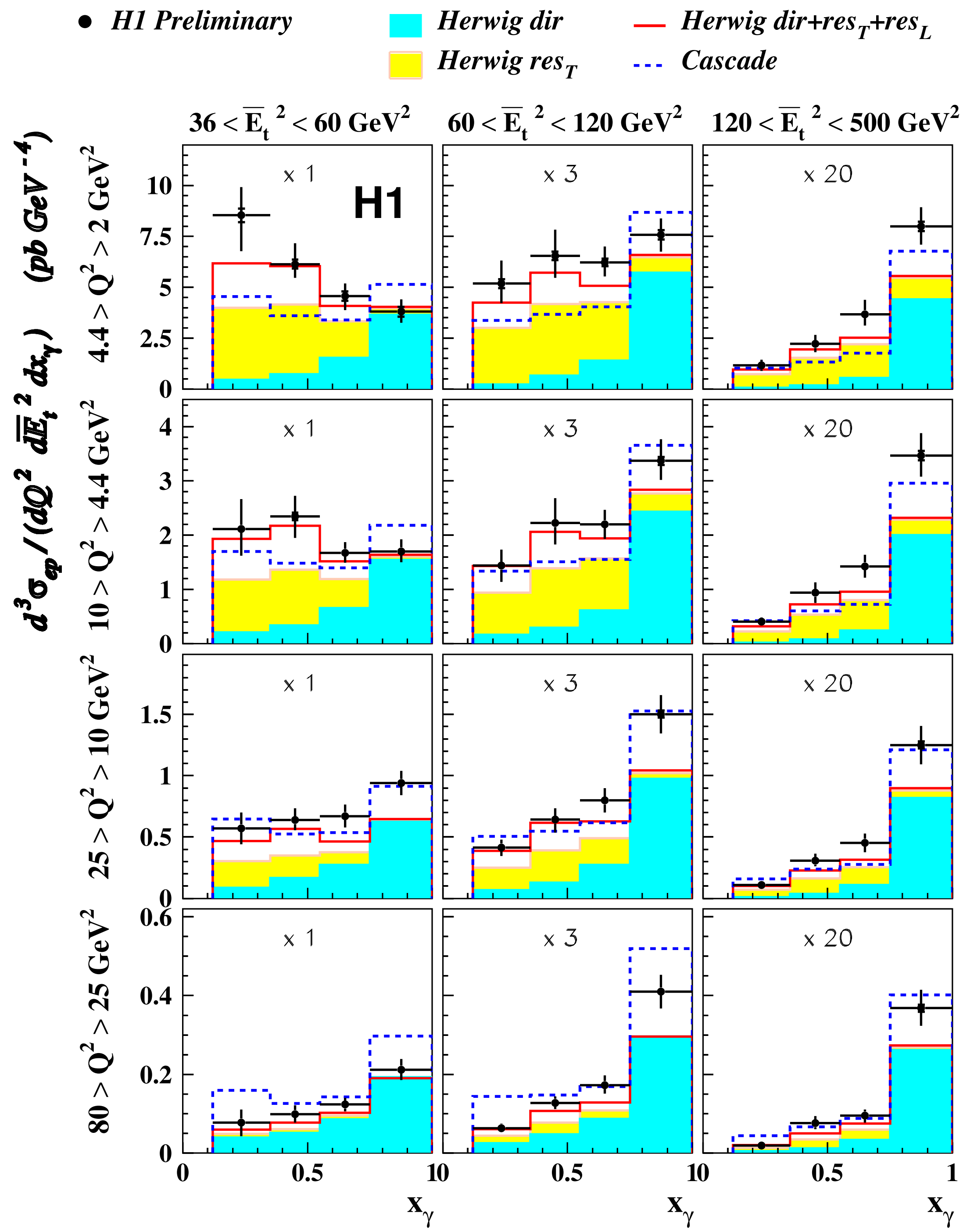

Figure 6: Triple differential dijet cross-section as a function of x_γ , $\overline{E}_t^2$ and Q^2. A combination of the theoretical predictions in Figure 4 and 5 is plotted here.

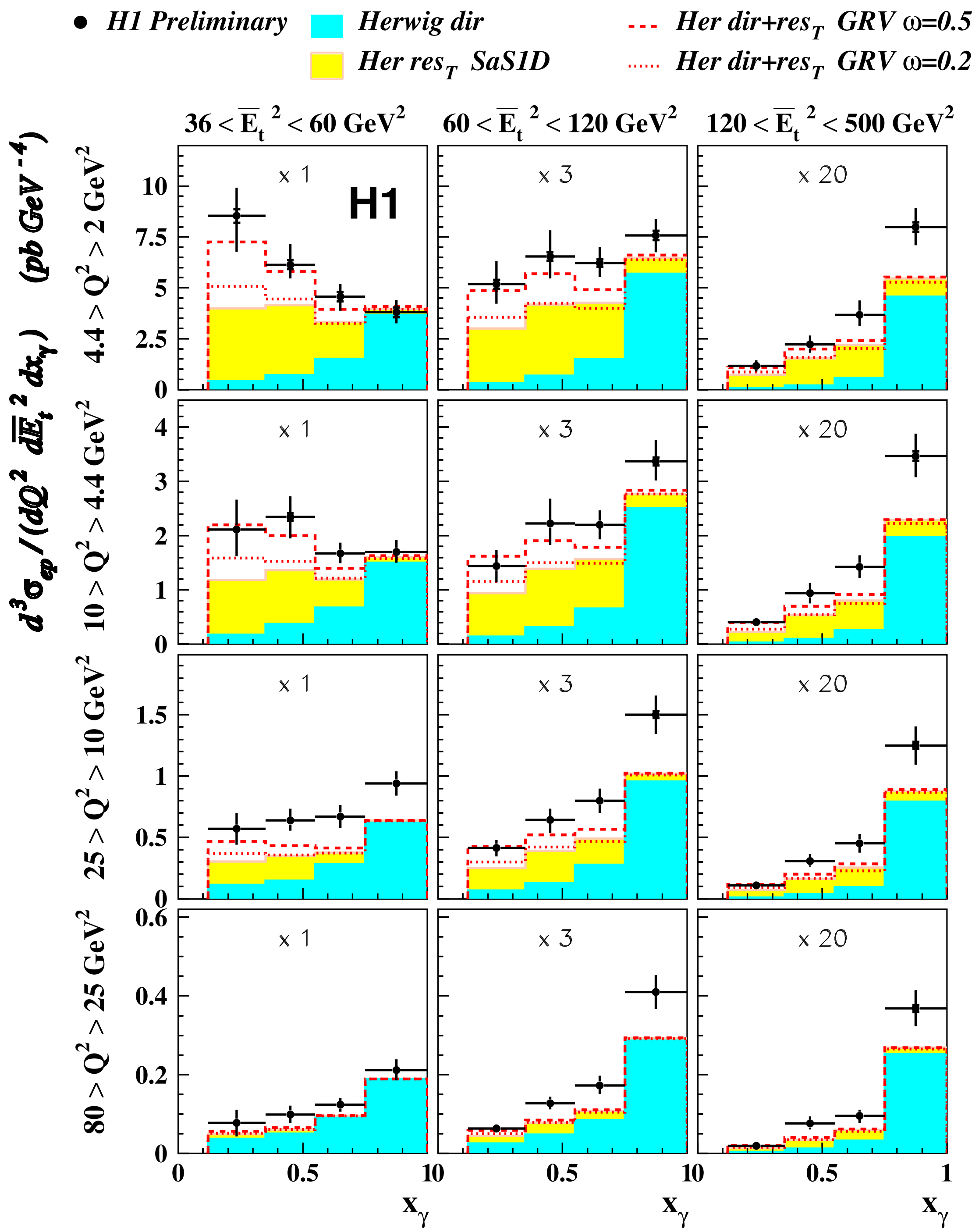

Figure 7: Triple differential dijet cross-section as a function of x_γ , $\overline{E}_t^2$ and Q^2. The data are compared to HERWIG with different γ_T^* PDFs. ω is a parameter from the Drees-Godbole factor [17], which suppresses the GRV γ PDFs with Q^2.

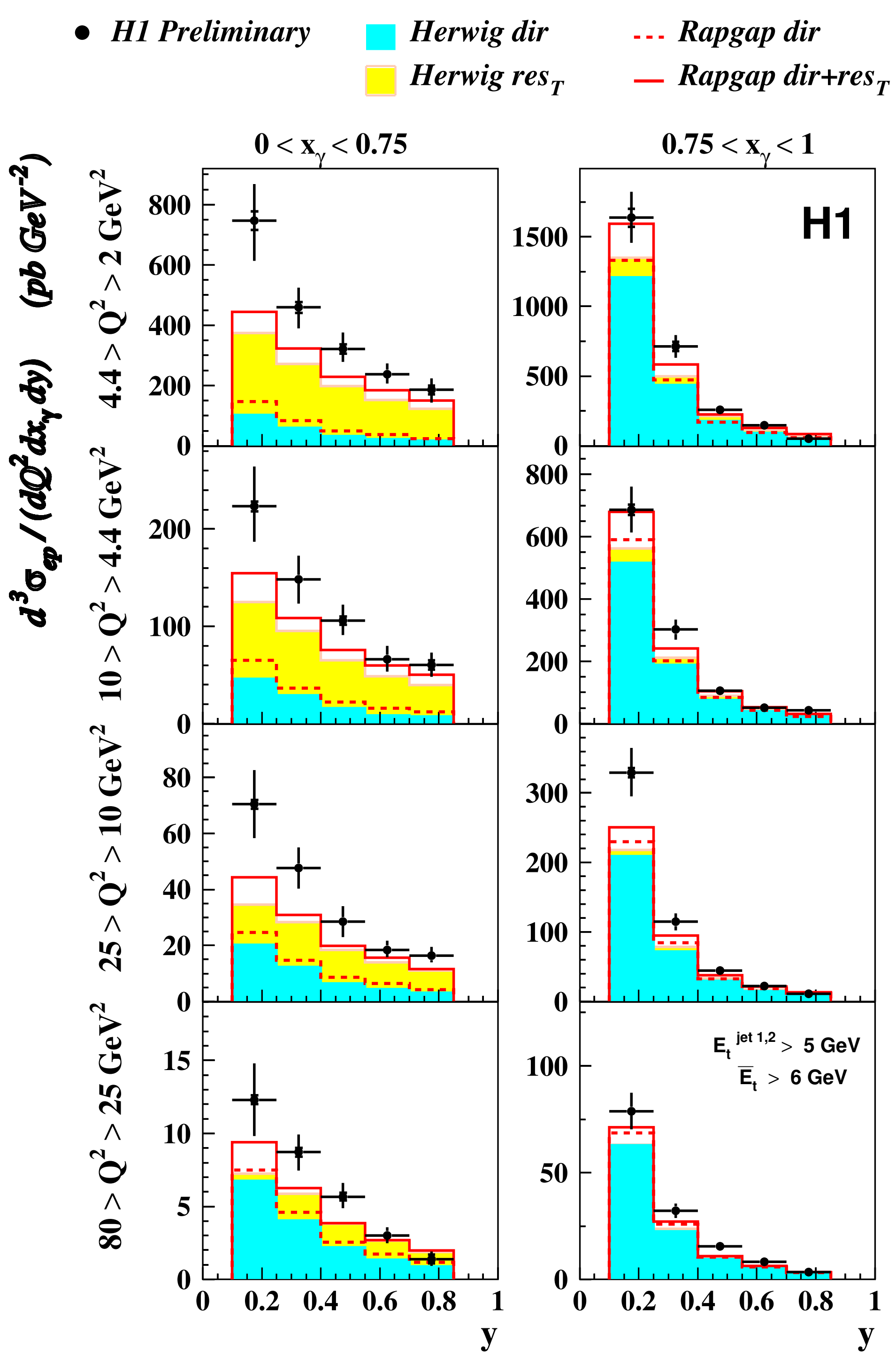

Figure 8: Triple differential dijet cross-section as a function of y, x_γ and Q^2. The data are compared to HERWIG and RAPGAP MC predictions. Both MC models underestimate the data, especially in the low x_γ and low y range.

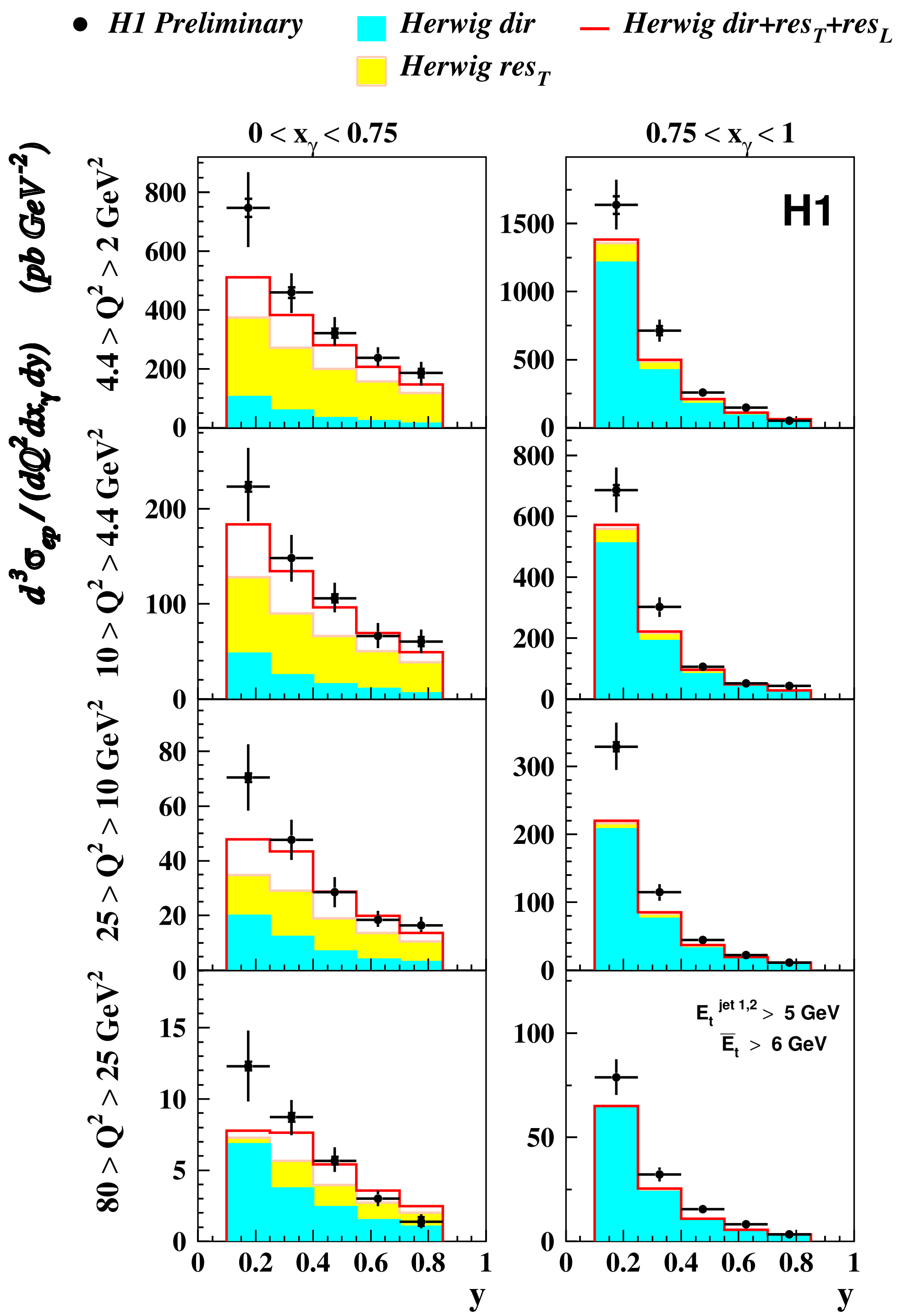

Figure 9: Triple differential dijet cross-section as a function of y, x_γ and Q^2. The data are compared to HERWIG with an additional contribution of the longitudinally polarized resolved photon processes. The additional longitudinal photon contributions lead to a better description of the slope of the y distribution.

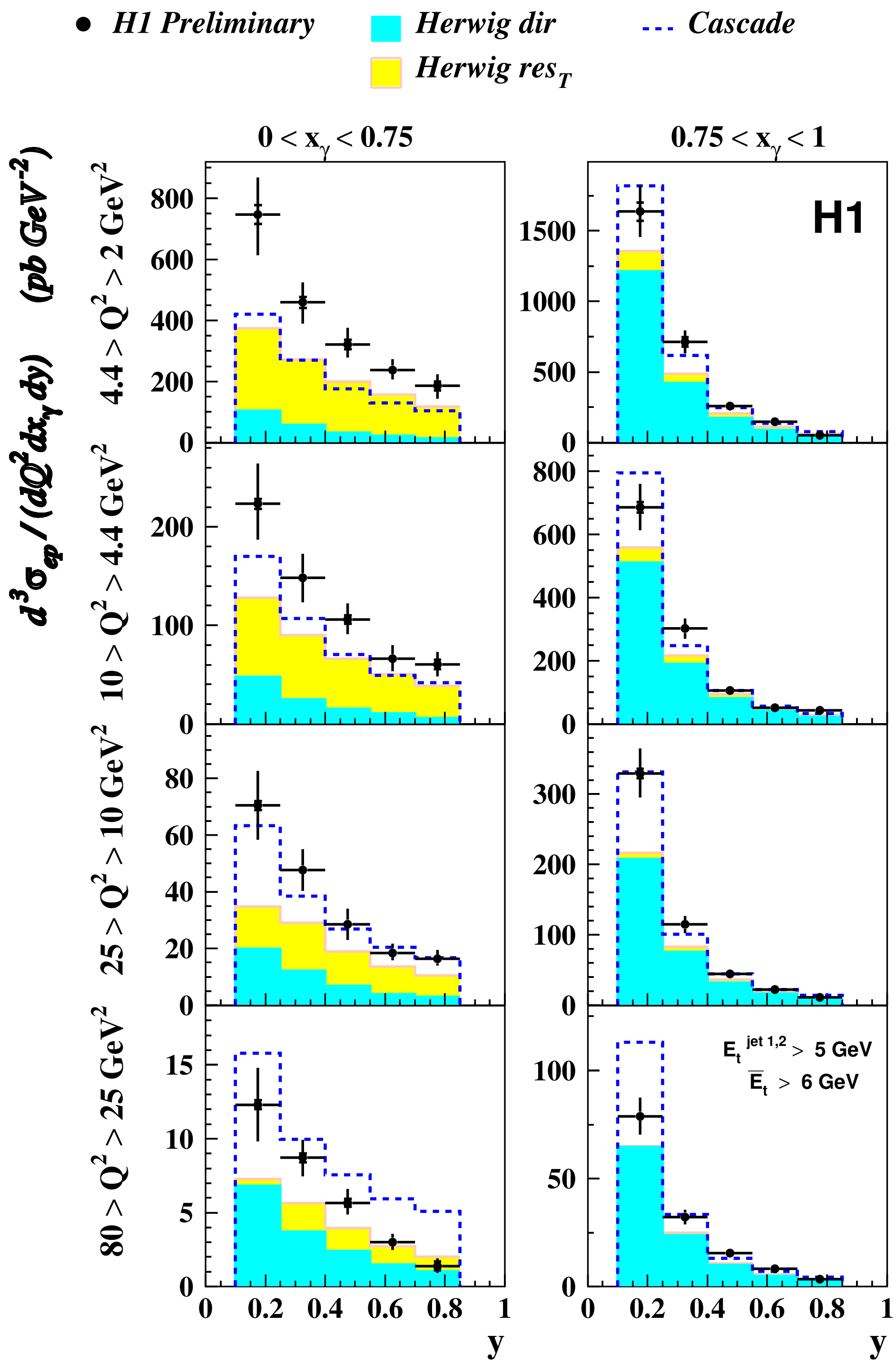

Figure 10: Triple differential dijet cross-section as a function of y, x_γ and Q^2. The data are compared to HERWIG and CASCADE MC models.

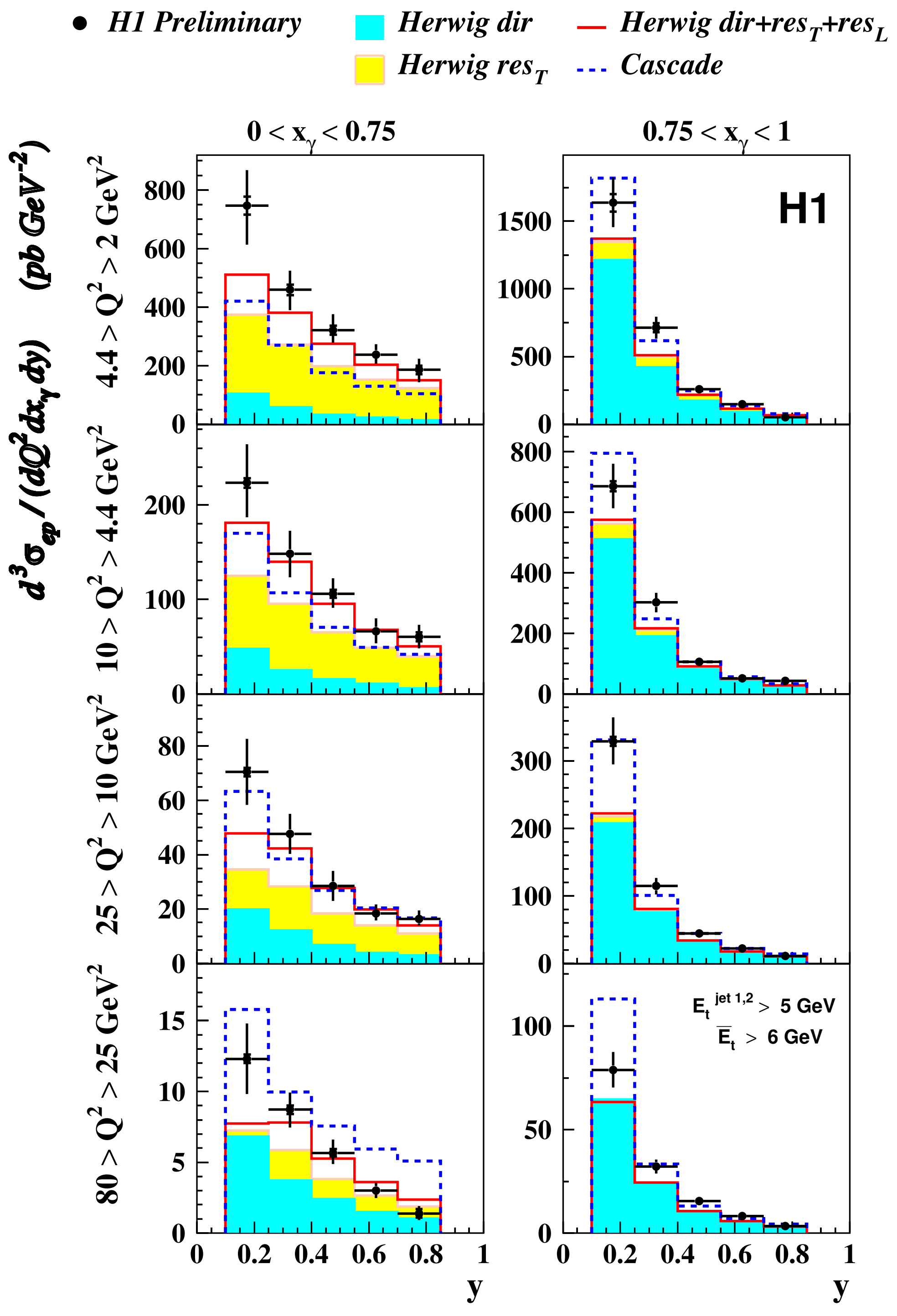

Figure 11: Triple differential dijet cross-section as a function of y, x_γ and Q^2. A combination of the model comparisons from Figure 9 and 10 is plotted here.

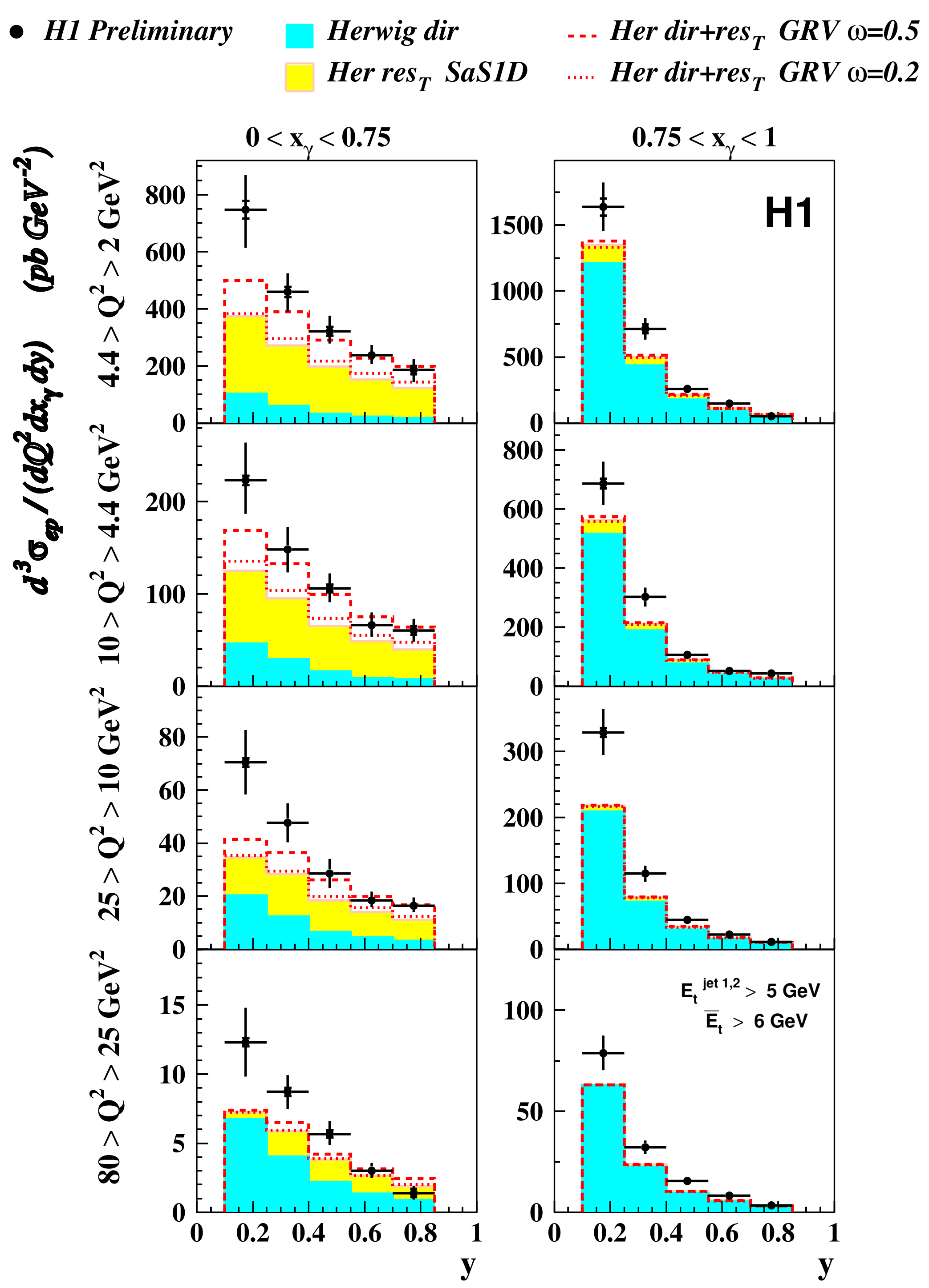

Figure 12: Triple differential dijet cross-section as a function of y, x_γ and Q^2. The data are compared to HERWIG with different γ^*_T PDFs (see caption to Fig. 7). The slope of y distributions are steeper in the data than in any of the HERWIG predictions plotted.

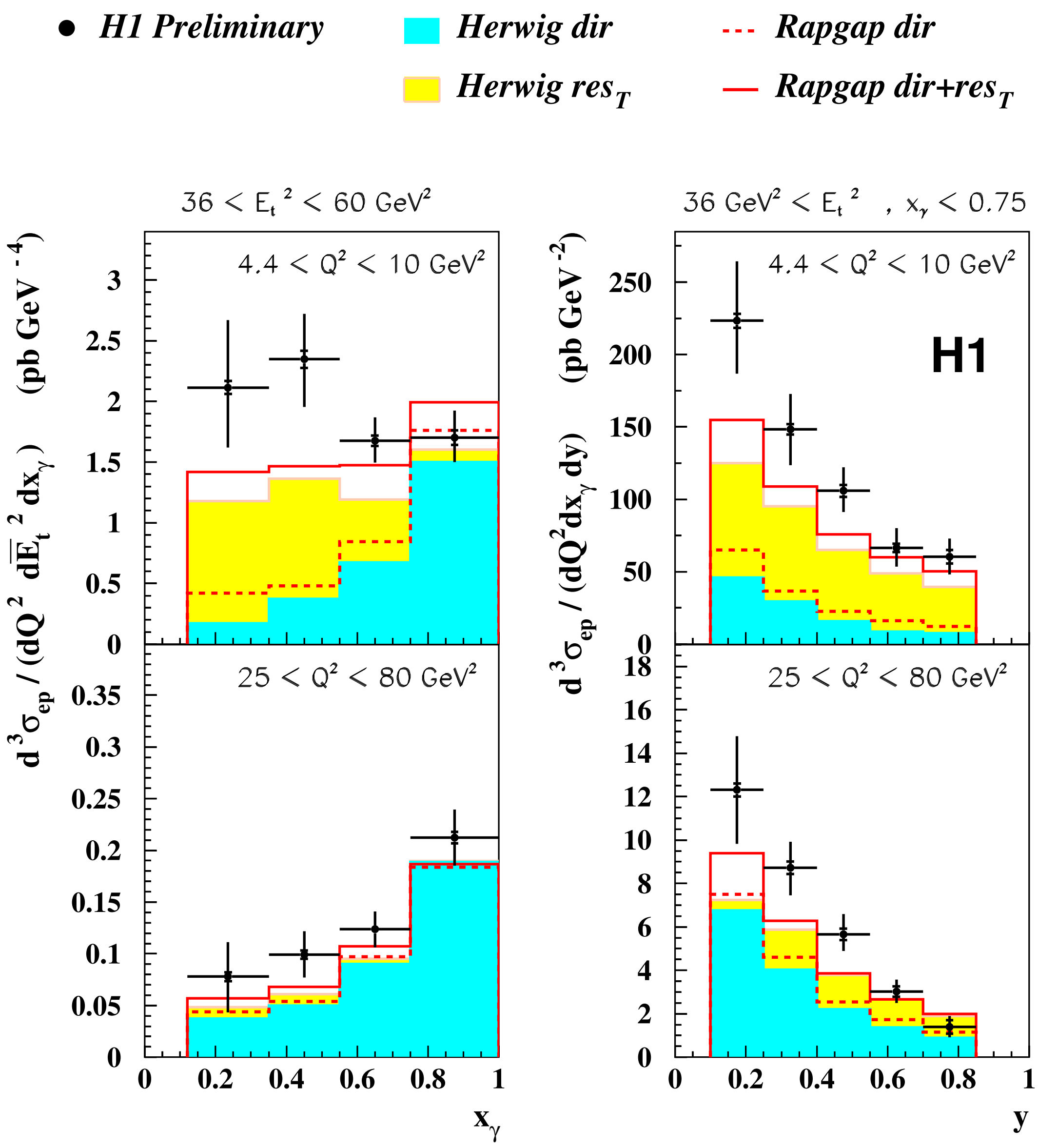

Figure 13: Simplified version of Fig. 3 and 8.

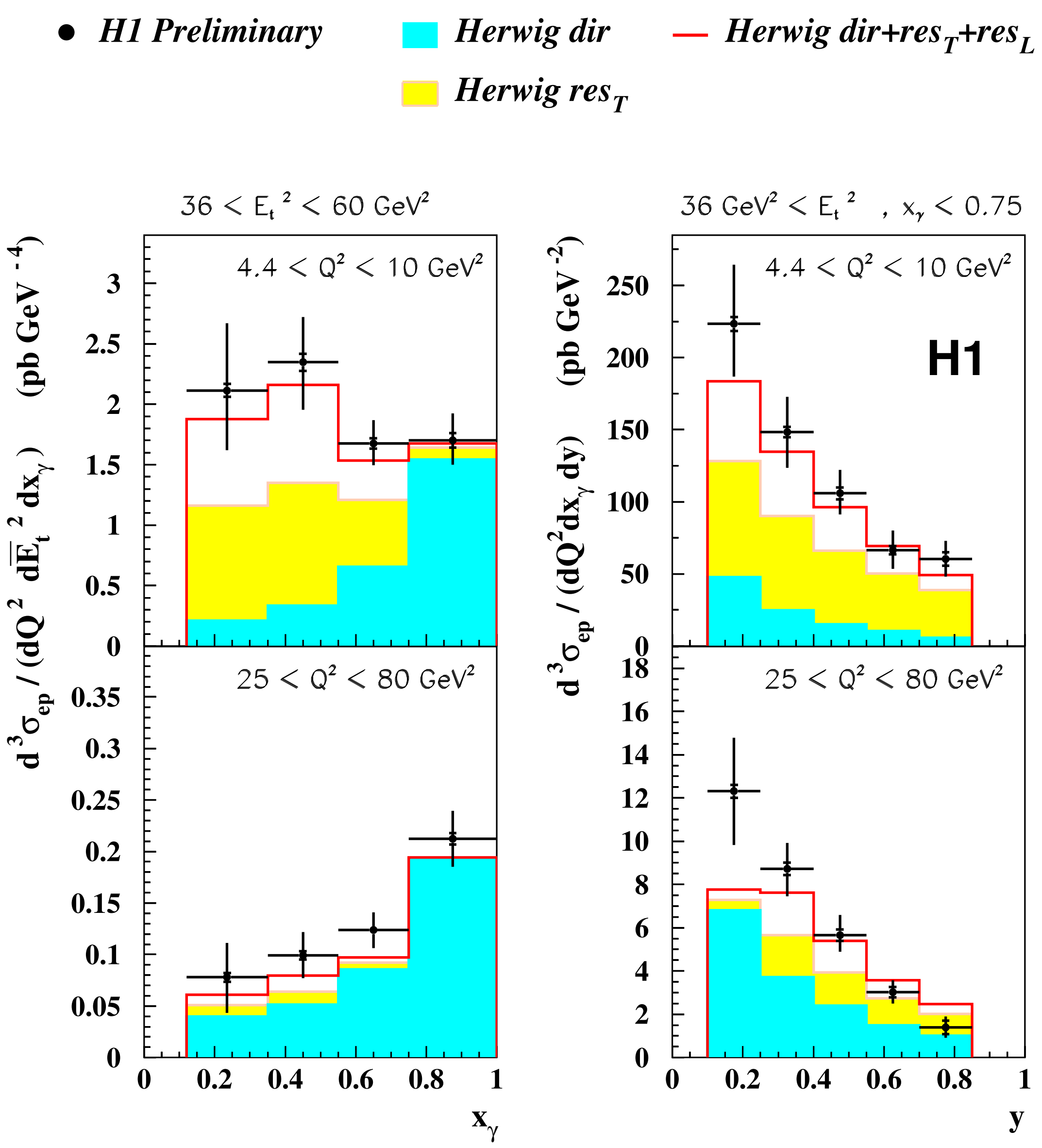

Figure 14: Simplified version of Fig. 4 and 9.

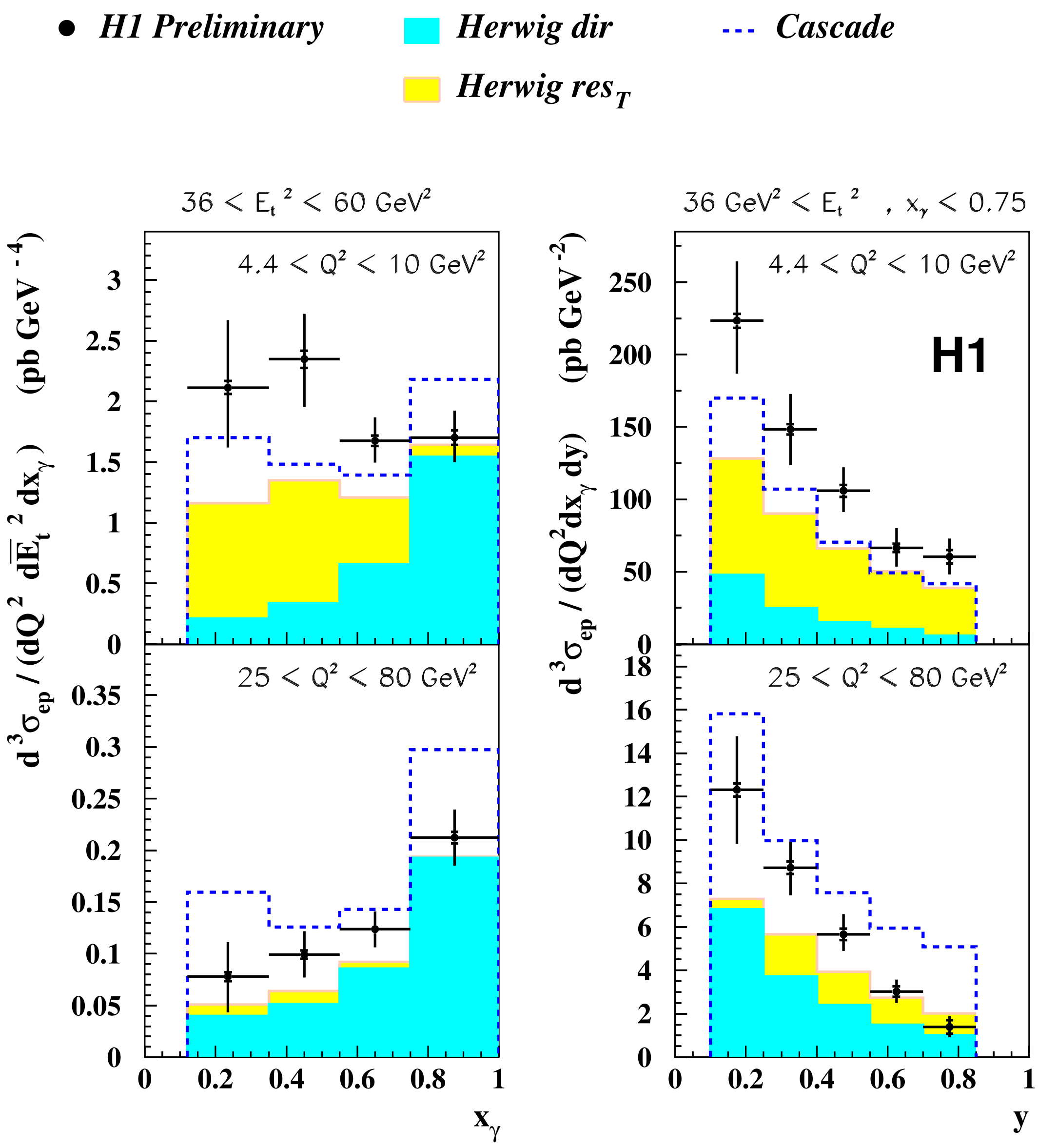

Figure 15: Simplified version of Fig. 5 and 10.

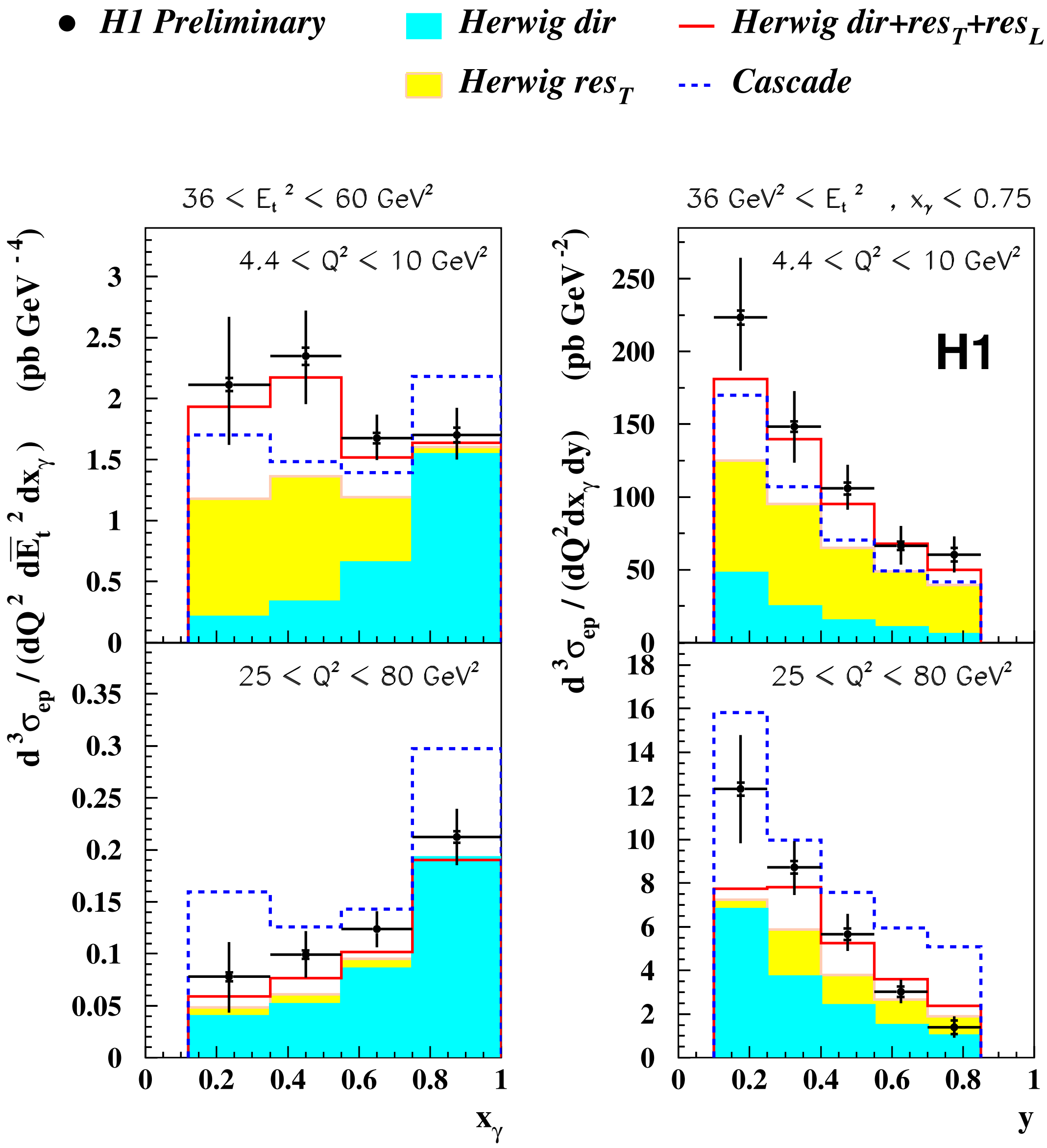

Figure 16: Simplified version of Fig. 6 and 11.

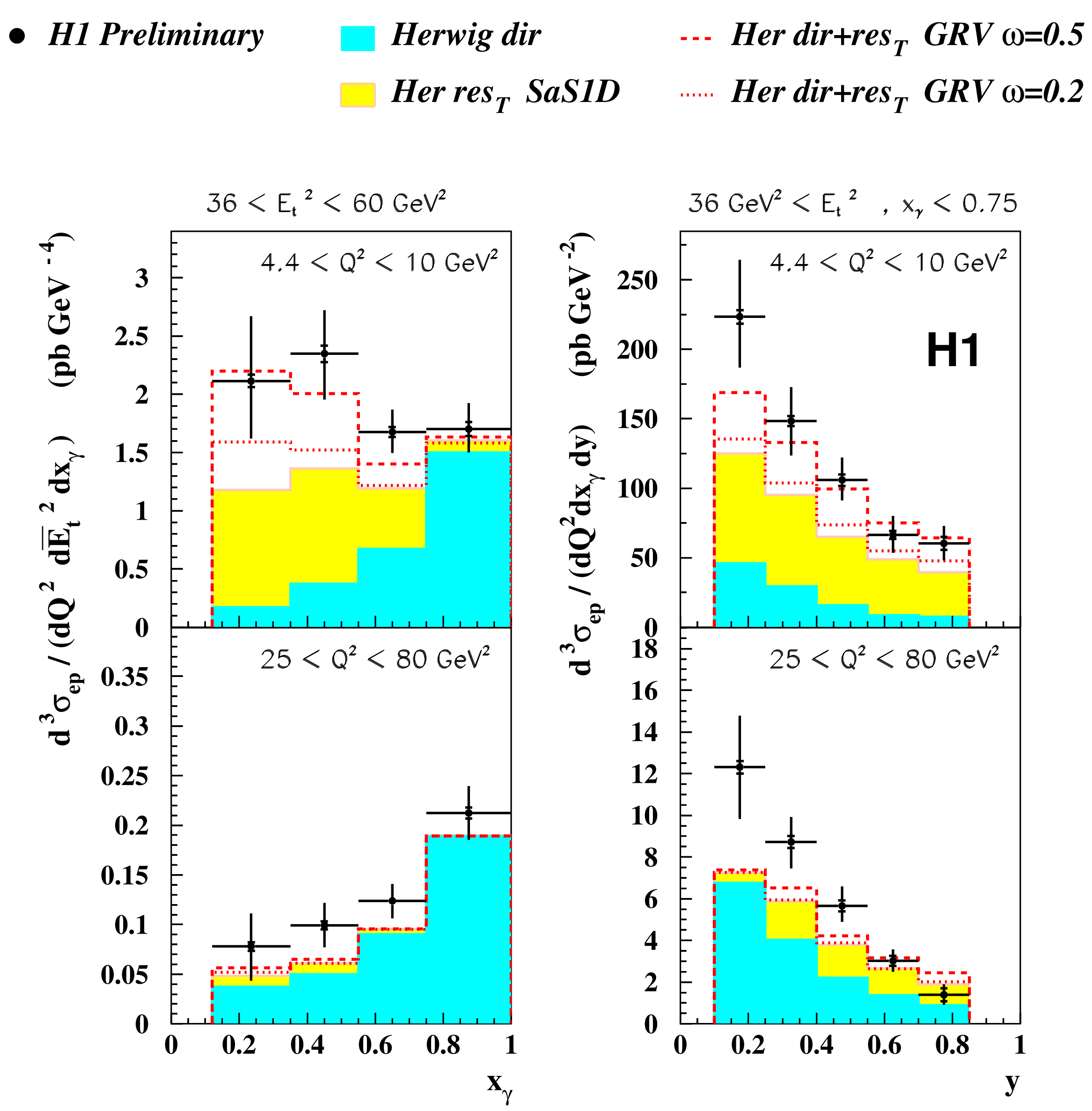

Figure 17: Simplified version of Fig. 7 and 12.